CrystEngComm

Accepted Manuscript

ROYAL SOCIETY OF CHEMISTRY

www.rsc.org/crystengcomm

Cite this: DOI: 10.1039/c0xx00000x

www.rsc.org/xxxxxx

PAPER

Controllable Synthesis of Ni Nanotube Arrays and Their Structure-Dependent Catalytic Activity toward Dye Degradation †

Xiang-Zi Li,[a,b] Kong-Lin Wu,[b] Yin Ye[b] and Xian-Wen Wei*[b]

Received (in XXX, XXX) Xth XXXXXXXXX 20XX, Accepted Xth XXXXXXXXX 20XX

DOI: 10.1039/b000000x

Ni nanotube arrays with an outer diameter of 100 nm to 2.0 μm were systematically fabricated through a novel facile one-step template-based electroless deposition method without any chemical modification. The structures of Ni nanotubes, such as inner and outer diameters, wall thickness, length, and crystalline state, can be well controlled by adjusting the template pores, reagent concentration, and gas evolution. Length-controlled Ni nanorods were obtained at a low reagent concentration in a time-dependent manner. The growth mechanisms, termed gas-directed-diffusion-assisted tubular growth and diffusion-directed clubbed growth, showed that both gas evolution and ionic diffusion rate were the key factor affecting the growth of Ni nanotubes (or nanorods). The relationship between the structures and catalytic properties of the as-prepared Ni nanostructures was studied in detail by dye degradation using $NaBH_4$ model reaction. Results showed that the Ni nanostructures exhibited higher catalytic efficiency for dye degradation than other nanocatalysts. In addition, the catalytic activities of these Ni nanostructures depended on both shape and size. The results of this study not only provide a general controllable synthesis approach for magnetic metal nanotube arrays but also promote promising nanocatalyst candidates for dye degradation.

Introduction

The development of nanotechnology and the increasing demand for novel functional materials have led to an increased scientific interest for the synthesis of nanostructures that exhibit different performances depending on a range of factors. [1–6] Previous studies have combined the template-assisted method with electrodeposition, electroless deposition, wetting chemical, atomic layer deposition, etc. to fabricate one-dimensional (1D) magnetic metal nanostructures, such as Fe, Co, Ni, and their alloys. [7–13] However, tubular metal nanostructures or their arrays are still difficult to obtain through the template-assisted approach. Despite the efforts exerted by scholars in the last decade, special strategies and techniques, including channel chemical modification, [7] triblock-copolymer-assist, [8] activation treatment, [10] high current density, [14] multistep template replication, [15] mercury cathode, [16] and precursor usage, [17] remain necessary. Furthermore, controlling and designing metal nanotubes are difficult through the template-assisted method, especially when combined with electroless deposition. Thus, the controllable synthesis and property of metal nanotubes with adjustable size and shape remain challenging.

a Department of Chemistry, Wannan Medical College, 241002 Wuhu (China) E-mail: lixiangzi@wnmc.edu.cn

b College of Chemistry and Materials Science, Key Laboratory of Functional Molecular Solids, the Ministry of Education, Anhui Laboratory of Molecule-based Materials, Anhui Normal University, 241000 Wuhu (China) Fax: +86 553-3869303; E-mail: xwwei@mail.ahnu.edu.cn

† Electronic Supplementary Information (ESI) available: See DOI: 10.1039/b000000x/

The physical and chemical properties of nanostructures are dependent on structural properties, such as size, shape, and crystalline state. Several studies have reported that the catalytic performance of nanostructures is strongly dependent on shape and size because of the different surface areas or crystal facets of nanostructures. [3, 18–23] In addition, the structure-dependent effect of metal nanostructures has elicited increased interest, accompanied by the development of the structure-controlled synthesis technique for metal nanostructures. Novel porous or hollow nanomaterials, including metals, [24–27] metal oxides, [28–30] and composites, [31–33] exhibit good catalytic properties because of their double surface area and high porosity. The catalytic performance of porous or hollow metal nanomaterials is significantly affected by their structures. However, only a few reports have focused on the catalytic performance of hollow tubular nanostructures, especially the structure–performance relationship of magnetic metal nanotubes.

In this study, we describe a simple chemical deposition method using polycarbonate (PC) templates to design and directly synthesize porous Ni nanoparticle nanotube arrays without any chemical modification, and mainly focus on the controllable synthesis technique firstly. In contrast to the anodic aluminum oxide template used in our previous study for 1D nanotube fabrication, [11] PC membrane templates not only can fabricate some metal nanotubes, [10, 34–38] but also have other advantages including their nanoscale pores easily obtained via the track-etched technique, optional specifications, lower cost, and easy removal by organic solvents, such as $CHCl_3$. Moreover, the outer diameters and lengths of Ni nanotubes can also be determined accurately by

the pore diameters and thicknesses of PC templates. Compared with previously reported catalysts, the as-prepared Ni nanotubes showed higher catalytic activities for dye degradation at room temperature by simple mixing. In particular, a good structure–performance relationship was established. These nanotubes can be employed in different applications in organic sewage treatment because of their remarkable performance.

Experimetal procedures

Preparation of Ni Nanostructures

Polycarbonate millipore isopore membrane filters (Whatman Inc.) were used as templates with specified pore diameters of 2.0, 0.2, 0.05, and 0.015 μm. The Ni nanotubes were prepared by a template-based electroless process as previously described [11]. Two glass utensils were used as bath with a PC membrane mounted in between. Fresh $NaBH_4$ and $NiSO_4$ aqueous solutions were prepared with oxygen-free distilled water, and then injected into each glass utensil individually. All reagents used in the experiment were of analytical purity. Electroless deposition was conducted at room temperature at different time. After deposition, the as-prepared PC membranes filled with Ni were polished with sand paper, dissolved, and then washed with $CHCl_3$ to drastically remove the PC template. Some black solids were obtained by centrifugal separation, and then dried in vacuum for further analysis. The corresponding Ni nanotube arrays were obtained after the as-prepared PC membranes filled with Ni were dissolved and washed with $CHCl_3$ directly without polish.

Characterization

The morphologies of the Ni Nanostructures were observed by scanning electron microscopy (SEM, Japan, Hitachi S-4800), transmission electron microscopy (TEM, Japan, JEM-2010), and selected-area electron diffraction (SAED) attached to TEM. The structure of the nanotubes was characterized by X-ray diffraction (XRD, Shimadzu, XRD-6000) pattern. The component of the nanotubes was tested by energy depressive X-ray spectroscopy (EDS, Japan, Hitachi S-4800) attached to SEM and X-ray photoelectron spectroscopy (XPS, Thermo Escalab 250). The UV–vis absorption spectra were measured at room temperature on a Hitachi U4100 spectrophotometer using solutions in a 1 cm quartz absorption cell.

Catalytic Degradation of Dyes

The degradations of three dyes (MO, MB, and RhB) by an excess of $NaBH_4$ were chosen as the model reaction in water. The catalytic redox reaction process was set up in a standard quartz absorption cell. Initially, freshly prepared $NaBH_4$ aqueous solution (1.0 mL, 6×10^{-2} M) was added to the quartz cuvette containing dyes (1.0 mL, 3×10^{-5} M) at room temperature, then approximately 1.0 mL of aqueous Ni nanotubes (100 mg/L) was added. The reaction mixtures were analyzed immediately by UV–vis absorption spectroscopy at room temperature. Moreover, the three dyes, corresponding reagent blank (without dyes), and sample blank (without catalyst) were also analyzed by UV–vis absorption spectroscopy.

Results and discussion

The XRD pattern of the as-synthesized Ni nanotubes obtained by 0.2 μm PC membrane is shown in Fig. S1a (see ESI). The diffraction pattern exhibited weak peaks at 2θ = 44.5, 51.9, and 76.6°, corresponding to the (111), (200), and (220) plane of face-centered cubic Ni (JCPDS 70-0989), which showed that the as-prepared nanotubes maybe weak polycrystalline in structure. The EDS result also confirmed that the nanotubes were primarily composed of nickel (Fig. S1b), and the peak of oxygen can attribute to the nanotube surface oxidation. The element composition of the nanotubes were also verified by the XPS spectrum (Fig. S1c), which displayed the peaks of Ni $2p_{3/2}$ (853.2 eV) and Ni $2p_{1/2}$ (870.9 eV), which was agreement with the zero valence of Ni. Moreover, the peaks at 191.9 eV shown in Fig. S1d can be attributed to the binding energy of B 1s, which showed the existence of the B-O bond. All the above results were also similar to that of our previous work. [11]

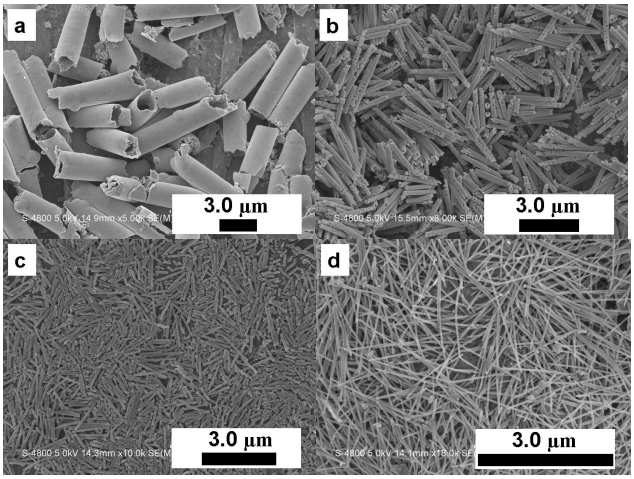

Fig. 1 SEM images of Ni nanotubes (nanorods) obtained in PC membrane with different template pore diameter: (a) 2.0, (b) 0.2, (c) 0.05, and (d) 0.015μm.

The template-based chemical reduction processing of aqueous $NiSO_4$ solution enabled the synthesis of Ni nanotubes (nanorods) with different sizes depending on the template pores, reagent concentration, gas evolution, and reaction time.

Template pore diameters significantly affect nanostructures. Thus, the synthesis of Ni nanotubes with different PC membranes was investigated. Fig. 1a to 1d show the typical SEM images of the Ni nanotubes (nanorods) obtained by electroless deposition in PC membrane with different template pore diameters (2.0, 0.2, 0.05, and 0.015 μm). The same reagent concentration [C ($NaBH_4$) =1.0 M, C (Ni^{2+}) =0.5 M] and deposition time (150 s) were used during the reaction. Nonetheless, the lengths of the nanotubes obtained were markedly different because the different specifications PC membranes were used. Moreover, the lengths of the nanotubes were shorter than the thickness of the corresponding PC membrane which was attributable to the different reaction conditions and ultrasonic treatment. The outer diameter, wall thickness, and crystal structure of the nanotubes

can be clearly observed from the TEM images (Fig. 2a to 2c), wherein the tubular nanostructures are apparent. Furthermore, the nanotubes were composed of numerous nanoparticles called nanoparticle nanotubes, [39] and mostly polycrystalline in structure (inset of Fig. 2a) which was according with that of XRD. A large number of Ni nanorods were obtained when using the PC membrane with a pore diameter of 0.015 μm. As shown in Fig. 1d and 2d, the outer surface of the Ni nanorods was illegibility, but their SAED patterns displayed numerous diffraction dots (inset of Fig. 2d). Therefore, the as-prepared Ni nanorods had better crystallinity than the above obtained Ni nanotubes, although both types had polycrystalline structures.

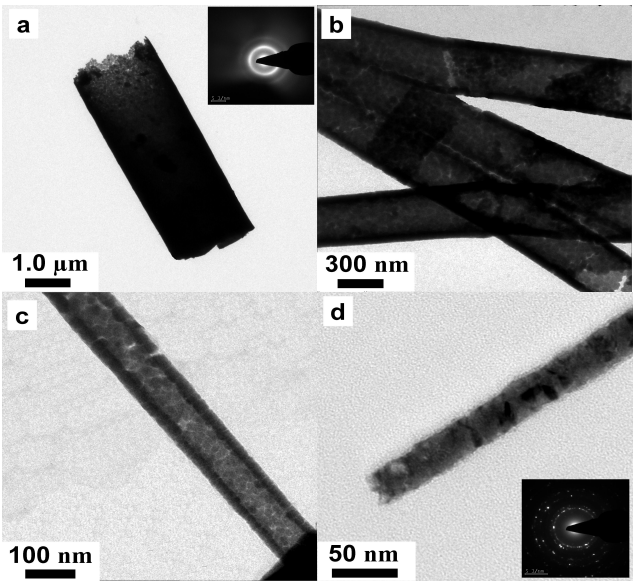

Fig. 2 TEM images of Ni nanotubes (nanorods) obtained in PC membrane with different template pore diameter: (a) 2.0, (b) 0.2, (c) 0.05, and (d) 0.015μm. Inserts are SAED patterns

The detailed data on the sizes of the Ni nanotubes mediated by the different PC membranes are shown in Tab. 1. The outer diameter of the Ni nanotubes (nanorods) was larger than the pore diameter of the corresponding PC membrane, especially for the small-pore PC membrane, because the actual pore diameters of commercial PC membranes are generally larger compared with the quoted pore diameters. [5] Furthermore, the wall thickness, average tube length, and nanoparticle diameter decreased as the template pore diameter decreased. However, the diameter of the Ni nanorods (30 nm) obtained from the PC membrane with a pore diameter of 0.015 μm was similar to the wall thickness (25 nm) of the Ni nanotubes obtained from the PC membrane with a pore diameter of 0.05 μm. As a result, the hollow structure and surface nanoparticles both disappeared. Thus, these structures are more appropriately called Ni nanorods. The actual deposition time in the pores could be different for the four above-mentioned PC membranes, although their actual reaction time was all 150 s, which is also an evidence of the growth mechanism of Ni nanotubes.

The gas-assisted evolution of the morphology of the Ni nanotubes was studied using different reagent concentrations. All experiments were conducted within 150 s using the PC membrane with a pore diameter of 0.2 μm. Fig. S2 shows the SEM images of the Ni nanotubes obtained at different concentrations of $NaBH_4$ and $NiSO_4$ (concentration ratio = 4.0 to 0.25). The products with similar outer diameters in ca. 280 nm were well dispersed and had rough surfaces. The SEM images of the products at decreasing concentration ratio [$C(BH_4^-)/C(Ni^{2+})$] showed that the product transformed from nanotubes (Fig. S2a to S2d) to nanorods (Fig. S2e to S2g) and back to nanotubes (Fig. S2h). As shown in Fig. S2b to S2d, the products had tubular structure and united length. Moreover, one side of the nanotubes was dark, whereas the other side was white, which showed that the wall thicknesses of the two sides of the nanotubes were different. However, one side of the nanotubes inconsistently became an aggregate of some nanoparticles (Fig. S2a and S2h), and their outer surfaces were also different from those of the Ni nanorods (Fig. S2e to S2g). The corresponding TEM images in Fig. S3 show the area where the wall thickness of the nanotubes can be clearly observed and confirm the presence of nanoparticles with different diameters.

Tab. 1 The detailed data of Ni nanotubes obtained in PC membrane with different template pore diameter (C ($NaBH_4$) = 1.0 M, C (Ni^{2+}) = 0.5 M, reaction time is 150 s.)

PC template Quoted pore diameter (μm)	As-obtained Ni nanotubes (nanorods)			
	Outer diameter (μm)	Wall thickness (nm)	Average Length (μm)	Ni particle diameter (nm)
2.00	2.00	180	6.3	40-50
0.20	0.28	49	2.5	25-30
0.05	0.10	25	1.2	13-22
0.015	0.03 [a)]	- [b)]	1.9	- [c)]

[a)] The diameter of Ni nanorods; [b)] Ni nanorods don't have wall thickness; [c)] The particles in the Ni nanorods surface are not obvious.

Tab. 2 Ni nanotubes fabricated in PC membrane with different concentrations of BH_4^- and Ni^{2+} (PC template pore diameter is 0.2 μm, reaction time is 150 s.)

No.	Initial concentration			Mirror formation		Ni Structures		
	$C(BH_4^-)$/M	$C(Ni^{2+})$/M	$C(BH_4^-)/C(Ni^{2+})$	BH_4^- side	Ni^{2+} side	shape	size d /nm [a)]	size L max /μm [b)]
1	1.00	0.25	4	no	yes	tube	72	2.9
2	1.00	0.50	2	no	yes	tube	49	3.8
3	0.50	0.25	2	no	yes	tube	80	5.0
4	0.50	0.50	1	no	yes	tube	63	7.4
5	0.25	0.50	0.5	faint	yes	tube	57	5.2
6	0.10	0.20	0.5	few	few	rods	-	2.9
7	0.05	0.10	0.5	faint	faint	rods	-	2.9
8	0.025	0.05	0.5	no	no	rods	-	1.8
9	0.125	0.50	0.25	few	yes	tube	69	2.8

[a] d is the wall thickness of the Ni nanotubes; [b] L is the length of the Ni nanotubes.

The combined SEM and TEM results (Fig. 2b, 3b, S2, and S3) on the reagent concentrations (0.025 M to 1.0 M), experimental phenomena, and morphological parameters of the products are summarized in Tab. 2. The high concentration of $NaBH_4$ or $NiSO_4$ (> 0.25 M), despite the change in the ratio of BH_4^- to Ni^{2+}, leaded to form Ni nanotubes easily (Nos. 1-5, 9 in Tab. 2). Decreasing the reagent concentration permitted the nanotubes to transform into nanorods with decreasing diameter at the same concentration ratio of 0.5 (Nos. 5-8), wherein a mixture of nanotubes and nanorods (No. 6) was also obtained (Fig. S2e). The results showed that reagent concentration was an important factor affecting nanotube or nanorod formation.

Some phenomena observed during template-based electrodeposition can provide powerful evidence to explain the controllable growth mechanism of the Ni nanotubes. First, gas evolution was apparent after adding $NaBH_4$ and Ni^{2+} solution into each glass utensil linked by PC membrane, respectively. Such evolution was proven to be a key factor affecting the formation of nanotubes. Moreover, the bubbles in the $NaBH_4$ solution were generally larger than those in the Ni^{2+} solution. Second, a layer of shiny Ni mirrors appeared only on the side of the $NiSO_4$ solution at the end of the reaction process, especially at higher reagent concentration (Nos. 1-4). On the other hand, a few Ni mirrors also appeared on the side of the $NaBH_4$ solution at lower reagent concentration (Nos. 5-7, 9). However, these Ni mirrors did not form on both sides of the PC membrane when the reagent concentration decreased further (No. 8). Moreover, very high (4) or very low (0.25) concentration ratios also resulted in a very compact Ni mirrors that were hardly removed with sand paper. The Ni nanotubes had a larger outer diameter and maximal length when the concentration of $NaBH_4$ was similar to that of $NiSO_4$ (No. 4). These results could be explained by the size confinement effect of nanochannels and the different ion diffusion rates.

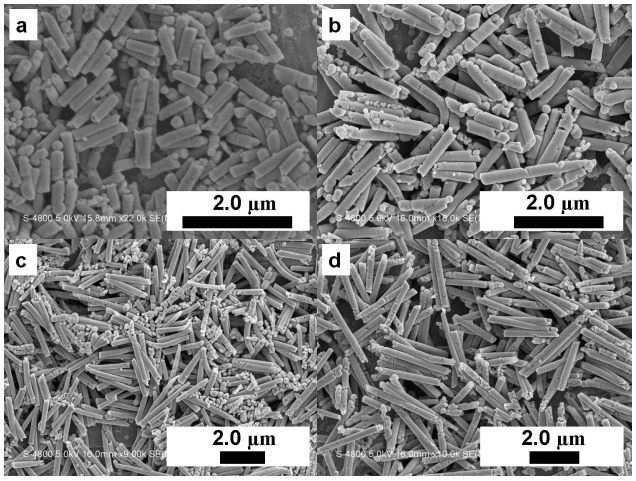

Fig. 3 SEM images of Ni nanorods obtained at different reaction time with PC membrane (template pore diameter is 0.2 μm, C ($NaBH_4$) =0.05 M, C (Ni^{2+}) =0.10 M): (a) 1 min, (b) 5 min, (c) 10 min, and (d) 30 min.

Ni nanotubes were consistently obtained at high reagent concentrations because of the formation of Ni mirrors, even when the reaction time was further prolonged. The time-dependent evolution of the size and morphology was further studied at a low reagent concentration (No. 7 in Tab. 2) to understand the growth process of Ni nanotubes and nanorods. The synthesis conditions for No. 7 were selected because the Ni mirrors were very faint, thereby forming unobstructed pores and allowing time-dependent reaction. The Ni nanorods were still the primary products even at a reaction time of 1 min (Fig. 3a and S4a) though the previous study found that nanotubes can be easily obtained at a short reaction time. [36] By contrast, prolonging the reaction time from 1 to 5, 10, and 30 min, the as-obtained products were purely nanorods with a similar outer diameter of 280 nm (Fig. S4b to S4d) and an increasing average length of 0.7, 1.7, 2.2, and 2.8 μm (Fig. 3a to 3d). Moreover, longer reaction time was associated with smoother nanorod surfaces. The as-prepared Ni nanorods were uniform when the reaction time was prolonged to 30 min (Fig. 3d). These results also illustrate that a low reagent concentration promotes the formation of solid nanorods.

We have studied the controllable growth of Ni nanotubes and obtained the following results. First, the pore diameter of the template had less important influence on the formation of Ni nanotubes during electroless deposition compared with the other factors. In this reaction system, the nanotubes were easily obtained unless the template pore diameter was very small, and the outer diameter of the Ni nanotubes was controllable in the range of 0.1 μm to 2.0 μm. These features make metal nanotubes superior over previous reports. It was found that both reagent concentration and gas evolution had important roles in the formation of nanotubes. The reactions resulting in Ni nanotube formation can be described by the following reactions: [40]

$$BH_4^- + 2H_2O = BO_2^- + 4H_2 \quad (1)$$
$$BH_4^- + 2Ni^{2+} + 2H_2O = 2Ni + BO_2^- + 4H^+ + 2H_2 \quad (2)$$
$$BH_4^- + H_2O = B + OH^- + 2.5H_2 \quad (3)$$

Higher reagent concentrations are associated with greater H_2 evolution, which has an important effect on the formation of nanotubes. [38, 41] By contrast, the confinement effects of the motion of molecules (or ions) in nanochannels or porous media are important and complicated. [42, 43] In a system composed of a nanochannel connecting two infinite chambers, the concentration gradient that develops along the nanochannel is classically described by the following equation:

$$c(x,t) = c_0 \mathrm{erfc}\left(\frac{x}{2\sqrt{Dt}}\right)$$

where c_0 is the concentration in an infinite reservoir, t is time, x is distance, and D is the diffusion constant. However, this equation must be modified based on concentration—a key factor affecting effective diffusivity. [44] This result was also validated that the ionic diffusion rate affected by concentration, pH, etc. [45] was the second most important factor affecting nanotube formation, which can cause the formation of Ni mirrors and seal the entrance of the pores to promote the sole formation of close-end nanotubes. As shown in Fig. 4, Ni nanotube arrays with different outer diameters can adhere to the Ni mirrors, and the mouths of the tubes were very clear.

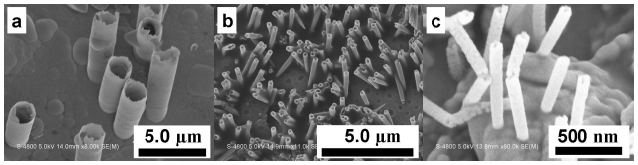

Fig. 4 SEM images of the different Ni nanotubes arrays onto the nickel mirror obtained by PC membrane with template pore diameter of (a) 2.0 μm, (b) 0.2 μm and (c) 0.05 μm.

Thus, the entire reaction process of Ni nanotube fabrication can be proposed as two categories mediated by different ionic diffusion rates of anions and cations (Fig. 5). (1) High ionic concentrations produce nanotubes. Under this condition, gas evolution is the dominant factor. Gas bubble can find a path through the pore center to the pore mouth, and anions and cations can rapidly enter the pores from two sides individually, which led to the preferential deposition of Ni atoms onto the inner wall because of the high activity of the inner wall and the block of gas path. Moreover, Ni mirrors form easily on one side of the pores because the ionic diffusion rate of anions (v_-) is much larger (or lower) than that of cations (v_+). The Ni mirrors shield the pore mouth of the PC template and ensure the formation of close-end nanotubes, which can be turned into open-end nanotubes by polishing with sand paper. We call this growth mechanism as gas-directed-diffusion-assisted tubular growth (GDDATG). (2) Low ionic concentrations produce nanorods. The generated H_2 is very weak and thus cannot form a gas path at the pore center. As a result, ionic diffusion becomes the dominant factor. Ni atoms can be deposited on both the center and wall of pores, thereby contributing to nanorod formation. In addition, the difference in the ionic diffusion rate of the anions and cations at low concentrations is minimal; thus, Ni mirrors can not form. The reduction reactions continue because the PC channels are still unblocked. Furthermore, the length of the Ni nanorods increase as the reaction time is prolonged. We call this growth mechanism as diffusion-directed clubbed growth (DDCG).

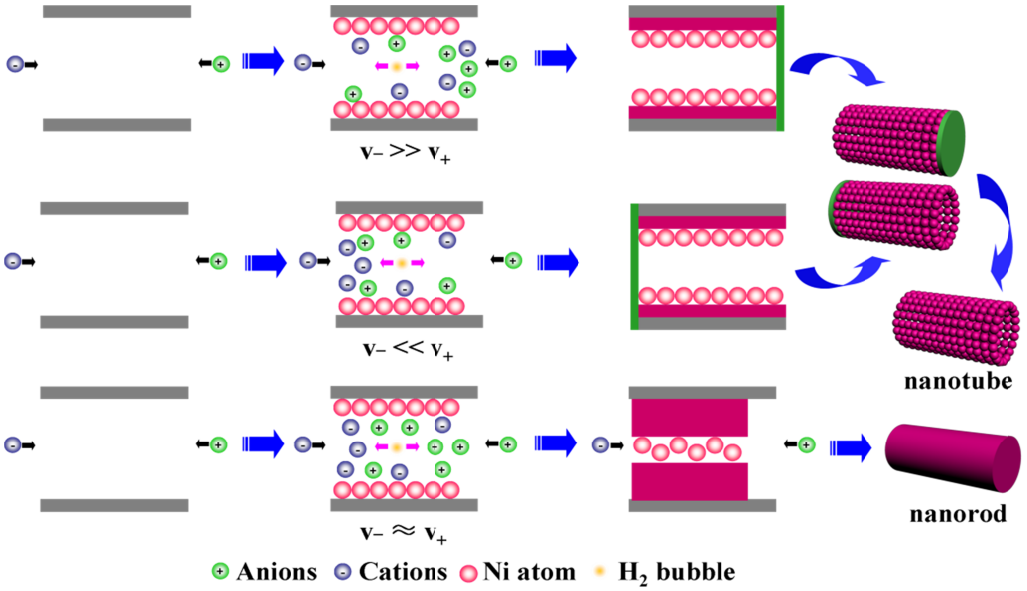

Fig. 5 Schematic illustration of the formation process for Ni nanotubes (Nanorods).

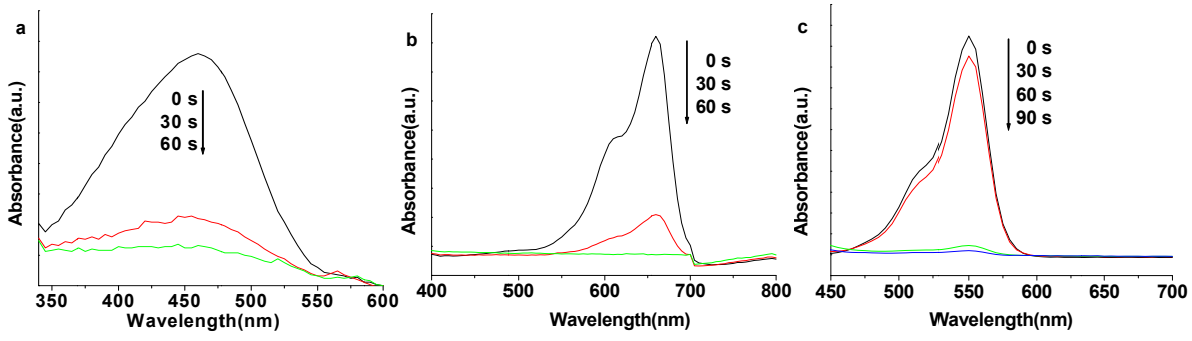

Fig. 6 UV-vis absorption spectra of (a) MO, (b) MB and (c) RhB degradation by $NaBH_4$ catalyzed by Ni nanotubes at room temperature.

The catalytic degradation of dyes by $NaBH_4$ was used as a simple model reaction to test the catalytic activities of the Ni nanotubes. This method was useful for analyzing the catalytic activities of metal nanostructures [46–50]. The degradation processes

of three dyes, including methyl orange (MO), methylene blue (MB), and rhodamine B (RhB), were monitored by time-resolved ultraviolet–visible (UV–vis) absorption spectra. Ni nanotubes with an outer diameter of approximately 280 nm were used as the preferential catalysts because of its higher output compared with the other nanotubes at the same reaction conditions. Upon the addition of a small amount of fresh $NaBH_4$ solution into the dye solutions in the presence of Ni nanotubes (280 nm), the characteristic absorption peaks of MO, MB, and RhB (460, 660, and 550 nm) rapidly decreased. After comparing with the UV-vis absorption spectra of the reagent blank and three dyes (Fig. S5 to S7), we found that the absorption peaks at 230 nm to 240 nm appeared with a concomitant disappearance of the peaks among 330 nm to 800 nm. This result indicated that the –N=N– or –C=N– bonds and π bonds of characteristic conjugated chromophores in dye molecules cleaved and that the degradation products still contained benzene rings [51, 52]. The primary wavelength ranges were studied at a scan speed of 2400 nm/min (Fig. 6) because the degradation time was extremely short. The dyes were observed to be degraded within approximately 60 s at room temperature using the Ni nanotube catalysts under the $NaBH_4$ model reaction, but the dyes didn't fade without the addition of $NaBH_4$ which excluded the physical adsorption role of nanotubes.

Tab. 3 The detailed data of the dyes degradation with $NaBH_4$ catalyzed by Ni nanotubes (280 nm) and other relevant nanomaterials.

Catalysts		Dyes		Final conc. of $NaBH_4$ (M)	t_0	k[a)]	*Ref.*
Type	Final mass dosage	Type	Final conc. (M)				
Ni nanotubes	33 mg/L	MO	1×10^{-5}	0.02	50 (s)	0.062 (s^{-1})[c)]	This work
		MB			60 (s)	0.037 (s^{-1})	
		RhB			80 (s)	0.013 (s^{-1})	
Hollow Cu microspheres	500 mg/L	MB	2×10^{-5}	0.02	8 (min)	-	25
Ag nanoparticles	0.00016 %[b)]	MO	7.8×10^{-5}	0.016 % W/V	9 (min)	-	53
CoO nanowires	0.25 mL	MB	8.0×10^{-6}	0.0175	81 (min)	0.0383 (min^{-1})	54
		RhB	8.0×10^{-6}	0.0175	22 (min)	0.143 (min^{-1})	

[a)] k is the first order rate constant; [b)] the concentration is mass per volume; c) Because an excess of $NaBH_4$ are used, pseudo-first-order kinetics with respect to the dyes reduction is set in this case to calculate the catalytic rate constant by the formula of $k = 0.693/t_{1/2}$ from Figs. S7b, S8b, and S9b.

Dye degradation by the $NaBH_4$ model reaction using other relevant nanomaterials is compared in Tab. 3. The degradation time of the Ni nanotube catalysts was significantly shorter than that of other nanomaterials because of the boron-doping, hollow, weak polycrystalline structures. [11] By contrast, the three dyes can hardly be reduced by $NaBH_4$ at similar reaction conditions when the as-prepared Ni catalysts were not added. These results suggest that the as-prepared Ni nanotubes are good candidates for highly efficient degradation of organic dyes in the presence of $NaBH_4$ and may have important applications in the field of environmental remediation.

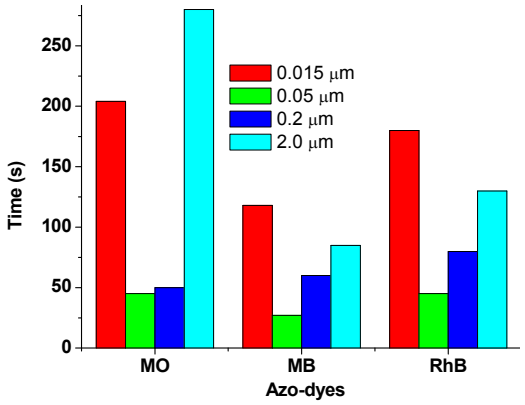

Fig. 7 Degradation time of three dyes (3×10^{-5} M) with $NaBH_4$ catalyzed by Ni nanotubes (nanorods, red) fabricated by PC membrane with four different quoted pores diameters.

The Ni nanotubes or nanorods with different diameters were used as catalysts for dye degradation at the same conditions to further investigate the structure–performance relationship of the as-prepared Ni nanostructures. The typical time-dependent degradation of MO, MB, and RhB are shown in Fig. S8 to S10. The Ni nanotubes (or nanorods) with different sizes showed different induction time (t_0). The detailed degradation time for three dyes is summarized in Fig. 7. All the as-prepared Ni nanotubes and nanorods exhibited high catalytic activity under the $NaBH_4$ model reaction for the degradation of MO, MB, and RhB. The diameters of the as-prepared Ni nanotubes were smaller, and the degradation time was shorter. This result can be attributed to the fact that Ni nanotubes with small diameters have high surface areas at the same catalytic concentration. However, the as-prepared Ni nanorods exhibited inferior catalytic properties even if they had a smaller outer diameter (30 nm) compared with the Ni nanotubes. This result maybe ascribed to the higher surface atom ratio of the nanoparticle-nanotubes compared with the nanorods and the easier surface oxidation for the very small Ni nanostructures. [55]

Conclusions

In summary, we reported a facile electroless deposition method for the controllable synthesis of Ni nanotubes with different sizes and shapes in a PC template. Notably, our magnetic metal nanotube fabrication method did't require any chemical modification of the template pores, which may reduce the possibility of introducing impurities. In our system, the morphological evolution from nanotubes to nanorods was systemically investigated using different reactants concentrations, reaction time, and templates. The effect of the reaction parameters on the final sizes of the Ni nanotubes was also explored in detail. The results provided insights into the growth mechanisms of GDDATG and DDCG, which exhibited competitive interaction of ion diffusion rate, gas evolution rate, and template pore diameter. We believe that the GDDATG mechanism can be used as a

general method for the growth of other metal and alloy nanotube arrays, through which some metal nanotubes, such as Fe, Co, and CoNi, have also been fabricated successfully. Finally, the catalytic properties of these Ni nanostructures were studied to determine the effects of structures on their catalytic degradation of dyes using $NaBH_4$. This general model reaction could make metal nanotube arrays a functional material platform for systematic studies of structure-dependent catalytic properties.

Acknowledgements

The authors thank the Natural Science Foundation of Anhui province of China (No. 1208085QE102), the National Natural Science Foundation of China (Nos. 21071005, 21271006), the Natural Science Foundation of Anhui Higher Education Institutions of China (Nos. KJ2013B305, KJ2010B250), the Foundation of Wuhu Science and Technology Plan (No. 2013cxy10), the Doctoral Research Initial Foundation of Wannan Medical College (No. 201221), the Innovation Funds of Anhui Normal University (No. 2011cxjj11) and the Research Culture Founds of Anhui Normal University (No. 2011rcpy038).

References

1 Z. X.Wu, W. Li, P. A.Webley and D. Y. Zhao, *Adv. Mater.*, 2012, **24**, 485–491.
2 M.Chen, B. H. Wu, J.Yang and N. F. Zheng, *Adv. Mater.*, 2012, **24**, 862–879.
3 M. H. Huang and P. -H. Lin, *Adv. Funct. Mater.*, 2012, **22**, 14–24.
4 X. W. Liu, D. S. Wang and Y. D. Li, *Nano Today*, 2012, **7**, 448–466.
5 W. Wu, X. H. Xiao, S. F. Zhang, J. Zhou, L. X. Fan, F. Ren and C. Z. Jiang, *J. Phys. Chem. C*, 2010, **114**, 16092–16103.
6 C. Z. Wu, H. Wei, B. Ning and Y. Xie, *Adv. Mater.*, 2010, **22**, 1972–1976.
7 J. C. Bao, C. Y. Tie, Z. Xu, Q. F. Zhou, D. Shen and Q. Ma, *Adv. Mater.*, 2001, **13**, 1631–1633.
8 F. -F. Tao, M. -Y. Guan, Y. Jiang, J. -M. Zhu, Z. Xu and Z. -L. Xue, *Adv. Mater.*, 2006, **18**, 2161–2164.
9 W. Lee, R. Scholz, K. Nielsch and U. Gösele, *Angew. Chem. Int. Ed.*, 2005, **44**, 6050–6054.
10 J. F. Rohan, D. P. Casey, B. M. Ahern, F. M. F. Rhen, S. Roy, D. Fleming and S. E. Lawrence, *Electrochem. Commun.*, 2008, **10**, 1419–1422.
11 X. Z. Li, K. L. Wu, Y. Ye and X. W. Wei, *Nanoscale*, 2013, **5**, 3648–3653.
12 K. Nielsch, F. J. Castaño, S. Matthias, W. Lee and C. A. Ross, *Adv. Eng. Mater.*, 2005, **7**, 217–221.
13 M. Daub, M. Knez, U. Goesele and K. Nielsch, *J. Appl. Phys.*, 2007, **101**, 09J111.
14 H. Q. Cao, L. D. Wang, Y. Qiu, Q. Z. Wu, G. Z. Wang, L. Zhang and X. W. Liu, *ChemPhysChem*, 2006, **7**, 1500–1504.
15 Q. T. Wang, G. Z. Wang, X. H. Han, X. P. Wang and J. G. Hou, *J. Phys. Chem. B*, 2005, **109**, 23326–23329.
16 X. Z. Li, X. W. Wei and Y. Ye, *Mater. Lett.*, 2009, **63**, 578–580.
17 T. N. Narayanan, M. M. Shaijumon, P. M. Ajayan and M. R. Anantharaman, *J. Phys. Chem. C*, 2008, **112**, 14281–14285.
18 K. P. Rice, A. E. Saunders and M. P. Stoykovich, *J. Am. Chem. Soc.*, 2013, **135**, 6669–6676.
19 R. Wang, H. He, L. –C. Liu, H. –X. Dai and Z. Zhao, *Catal. Sci. Technol.*, 2012, **2**, 575–580.
20 Z. Xu, F.-S. Xiao, S. K. Purnell, O. Alexeev, S. Kawi, S. E. Deutsch and B. C. Gates, *Nature*, 1994, **372**, 346–348.
21 J. Chen, Q. H. Zhang, Y. Wang and H. L. Wan, *Adv. Synth. Catal.*, 2008, **350**, 453–464.
22 H. Zhang, M. S. Jin, Y. J. Xiong, B. Lim and Y. N. Xia, *Acc. Chem. Res.*, 2013, **46**, 1783–1794.
23 W. Wu, R. Hao, F. Liu, X. T. Su and Y. L. Hou, *J. Mater. Chem. A*, 2013, **1**, 6888–6894.
24 M. Hakamada, F. Hirashima and M. Mabuchi, *Catal. Sci. Technol.*, 2012, **2**, 1814–1817.
25 J. W. Hong, S. W. Kang, B. –S. Choi, D. Kim, S. B. Lee and S. W. Han, *ACS Nano*, 2012, **6**, 2410–2419.
26 S. Y. Gao, X. X. Jia, J. M. Yang and X. Y. Wei, *J. Mater. Chem.*, 2012, **22**, 21733–21739.
27 L. X. Xia, H. P. Zhao, G. Y. Liu, X. H. Hu, Y. Liu, J. S. Li, D. H. Yang and X. F. Wang, *Colloid. Surf. A*, 2011, **384**, 358–362.
28 C. Guan, X. L. Li, Z. L. Wang, X. H. Cao, C. Soci, H. Zhang and H. J. Fan, *Adv. Mater.*, 2012, **24**, 4186–4190.
29 J. S. Luo, X. H. Xia, Y. S. Luo, C. Guan, J. L. Liu, X. Y. Qi, C. F. Ng, T. Yu, H. Zhang and H. J. Fan, *Adv. Energy Mater.*, 2013, **3**, 737−743.
30 M. T. Uddin, Y. Nicolas, C. Olivier, T. Toupance, L. Servant, M. M. Muller, H. -J. Kleebe, J. Ziegler and W. Jaegermann, *Inorg. Chem.*, 2012, **51**, 7764−7773.
31 J. Wu, Dr. L. W. Liao, W. S. Yan, Y. Xue, Y. F. Sun, X. Yan, Y. X. Chen and Y. Xie, *Chemsuschem*, 2012, **5**, 1207−1212.
32 Z. Y. Wang, D. Luan, C. M. Li, F. B. Su, S. Madhavi, F. Boey and X. W. Lou, *J. Am. Chem. Soc.*, 2010, **132**, 16271−16277.
33 L. X. Ding, A. L. Wang, G. R. Li, Z. Q. Liu, W. X. Zhao, C. Y. Su and Y. X. Tong, *J. Am. Chem. Soc.*, 2012, **134**, 5730−5733.
34 C. R. Martin, *Science*, 1994, **266**, 1961−1966.
35 S. H. Xue, C. B. Cao, D. Z. Wang and H. S Zhu, *Nanotechnology*, 2005, **16**, 1495.
36 K. Ž. Rožman, D. Pečko, L. Suhodolčan, P. J. McGuiness and S. Kobe, *J. Alloys Compd.*, 2011, **509**, 551−555.
37 G. Tourillon, L. Pontonnier, J. P. Levy and V. Langlais, *Electrochem. Solid-State Lett.*, 2000, **3**, 20−23.
38 D. M. Davis and E. J. Podlaha, *Electrochem. Solid-State Lett.*, 2005, **8**, D1− D4.
39 M. Lahav, T. Sehayek, A. Vaskevich and I. Rubinstein, *Angew. Chem. Int. Ed.*, 2003, **42**, 5576−5579.
40 Y. Zhu, X. K. Guo, Y. Q. Shen, M. Mo, X. F. Guo, W. P. Ding and Y. Chen, *Nanotechnology*, 2007, **18**, 195601.
41 Y. Fukunaka, M. Motoyama, Y. Konishi and R. Ishii, *Electrochem. Solid-State Lett.*, 2006, **9**, C62−C64.
42 I. D. Santo, F. Causa and P. A. Netti, *Anal. Chem.*, 2010, **82**, 997−1005.
43 G. Alì, M. Bisi, G. Spiga and I. Torcicollo, *Intern. J. Non-linear mechanics*, 2012, **47**, 769−776.
44 A. Ziemys, A. Grattoni, D. Fine, F. Hussain and M. Ferrari, *J. Phys. Chem. B*, 2010, **114**, 11117−11126.
45 J. Fu, S. Cherevko and C. –H. Chung, *Electrochem. Commun.*, 2008, **10**, 514−518.
46 M. Schrinner, M. Ballauff, Y. Talmon, Y. Kauffmann, J. Thun, M. Moller and J. Breu, *Science*, 2009, **323**, 617−620.
47 X. M. Zhao, B. H. Zhang, K. L. Ai, G. Zhang, L. Y. Cao, X. J. Liu, H. M. Sun, H. S. Wang and L. H. Lu, *J. Mater. Chem.*, 2009, **19**, 5547–5553.
48 Y. X. Zhang, H. L. Ding, Y. Y. Liu, S. S. Pan, Y. Y. Luo and G. H. Li, *J. Mater. Chem.*, 2012, **22**, 10779–10786.
49 S. W. Cao, J. Fang, M. M. Shahjamali, Z. Wang, Z. Yin, Y. H. Yang, F. Y. C. Boey, J. Barber, S. C. J. Loo and C. Xue, *CrystEngComm*, 2012, **14**, 7229–7235.
50 D. Jana and G. De, *RSC Adv.*, 2012, **2**, 9606–9613.
51 L. X. Wang, J. C. Li, Z. T. Wang, L. J. Zhao and Q. Jiang, *Dalton Trans.*, 2013, **42**, 2572–2579.
52 M. N. Nadagouda, I. Desai, C. Cruz and D. J. Yang, *RSC Adv.*, 2012, **2**, 7540–7548.
53 N. Gupta, H. P. Singh and R. K. Sharma, *J. Mol. Catal. A-Chem.*, 2011, **335**, 248–252.
54 S. Kundu, M. D. Mukadam, S. M. Yusuf and M. Jayachandran, *CrystEngComm*, 2013, **15**, 482–497.
55 H. Winnischofer, T. C. R. Rocha, W. C. Nunes, L. M, Socolovsky, M. Knobel, and D. Zanchet, *ACS Nano,* 2008, **2**, 1313–1319.

Graphical Abstract

Xiang-Zi Li, [a,b] Kong-Lin Wu, [b] Yin Ye, [b] and Xian-Wen Wei*[b]

[a] Department of Chemistry, Wannan Medical College, 241000 Wuhu (China)
[b] College of Chemistry and Materials Science, Key Laboratory of Functional Molecular Solids, the Ministry of Education, Anhui Laboratory of Molecule-based Materials, Anhui Normal University, 241000 Wuhu (China) Fax: +86 553-3869303; E-mail: xwwei@mail.ahnu.edu.cn

Ni nanotube (nanorods) arrays with variable structures have been controllably fabricated by a novel facile one-step template-based electroless deposition method, and the GDDATG and DDCG growth mechanisms are introduced. The relationship of structures and catalytic properties for the Ni nanostructures are also studied, the as-prepared Ni nanostructres prsent higher catalytic efficiency for dye degradation.